Materials Research Letters
Publication details, including instructions for authors and subscription information:
http://www.tandfonline.com/loi/tmrl20

Layer Stability and Material Properties of Friction-Stir Welded Cu-Nb Nanolamellar Composite Plates

Josef Cobb[a], Shraddha Vachhani[b], Robert M. Dickerson[c], Patricia O. Dickerson[c], Weizhong Han[de], Nathan A. Mara[ce], John S. Carpenter[c] & Judy Schneider[a]

[a] Mechanical Engineering Department, Mississippi State University, Starkville, MI 39762, USA

[b] Mechanical Engineering Department, Georgia Institute of Technology, Atlanta, GA 30332, USA

[c] Materials Science and Technology Division, Los Alamos National Laboratory, Los Alamos, NM 87545, USA

[d] Center for Advancing Materials Performance from the Nanoscale, State Key Laboratory for Mechanical Behavior of Materials, Xi'an Jiaotong University, Xi'an 710049, People's Republic of China

[e] Center for Integrated Nanotechnologies, Los Alamos National Laboratory, Los Alamos, NM 87545, USA

Published online: 22 May 2014.

To cite this article: Josef Cobb, Shraddha Vachhani, Robert M. Dickerson, Patricia O. Dickerson, Weizhong Han, Nathan A. Mara, John S. Carpenter & Judy Schneider (2014): Layer Stability and Material Properties of Friction-Stir Welded Cu-Nb Nanolamellar Composite Plates, Materials Research Letters, DOI: 10.1080/21663831.2014.918567

To link to this article: http://dx.doi.org/10.1080/21663831.2014.918567

MATERIALS RESEARCH LETTERS

Mater. Res. Lett., 2014
http://dx.doi.org/10.1080/21663831.2014.918567

Taylor & Francis
Taylor & Francis Group

www.tandfonline.com/toc/tmrl20/current

Layer Stability and Material Properties of Friction-Stir Welded Cu–Nb Nanolamellar Composite Plates

Josef Cobb[a]*, Shraddha Vachhani[b], Robert M. Dickerson[c], Patricia O. Dickerson[c], Weizhong Han[d,e], Nathan A. Mara[c,e], John S. Carpenter[c] and Judy Schneider[a]

[a]*Mechanical Engineering Department, Mississippi State University, Starkville, MI 39762, USA;* [b]*Mechanical Engineering Department, Georgia Institute of Technology, Atlanta, GA 30332, USA;* [c]*Materials Science and Technology Division, Los Alamos National Laboratory, Los Alamos, NM 87545, USA;* [d]*Center for Advancing Materials Performance from the Nanoscale, State Key Laboratory for Mechanical Behavior of Materials, Xi'an Jiaotong University, Xi'an 710049, People's Republic of China;* [e]*Center for Integrated Nanotechnologies, Los Alamos National Laboratory, Los Alamos, NM 87545, USA*

(*Received 15 February 2014; final form 20 April 2014*)

Initial efforts to friction-stir weld (FSW) Cu–Nb nanolamellar composite plates fabricated via accumulative roll bonding are reported in this study. Parent material layers within the composite were nominally 300 nm and exhibited a hardness of 2.5 GPa. After FSW, two types of microstructures were present: a refined layered structure, and an equiaxed nanocrystalline microstructure with grain diameters on the order of 7 nm. The type of microstructure was dependent on location within the FSW nugget and related to varying amounts of strain. Material hardness increased with refinement, with the equiaxed microstructure reaching a maximum hardness of 6.0 GPa.

Keywords: Nanograin, Nanolayers, Friction-Stir Welding, Copper Niobium

Nanolamellar Cu–Nb bimetallic composites have been extensively studied due to their significantly higher strength and radiation damage tolerance as compared with their bulk counterparts.[1–7] These improvements are reported to increase as the layer thickness (h) decreases to the nanometer (nm) scale with a maximum strength occurring around a thickness of 2 nm.[2] These properties are reported to emanate from a combination of heterophase interface character (ω) and density (ρ), with the strength largely dominated by ρ.[5,6] Cu–Nb nanolamellar bimetallic composites have been studied for materials produced via two fabrication routes: physical vapor deposition (PVD) [4] and accumulative roll bonding (ARB).[8–10] While the PVD method can currently only produce a small volume of laboratory scale material, the ARB process allows the production of much larger volume, engineering-scale quantities of material.[5,9] Previous studies indicate that ρ can be controlled and ω stabilized during ARB processing via manipulation of processing parameters.[10] Thus, ARB opens the door for the fabrication of nanocomposite materials with properties tailored for specific applications via industry scalable manufacturing techniques. To further realize this goal, the stability of ω and ρ under commercially available joining processes must be understood. Friction-stir weld (FSW), a solid-state joining process, is explored as a possible joining process for maintaining high ρ and hence the strength of the material within the weld region. Simulations show that the stability of ω, observed in previous studies,[7,11,12] is derived from the ability of specific interfacial structures to accommodate the plastic deformation of the ARB process. Since the FSW process will introduce additional severe plastic deformation in a manner that differs considerably from that used to synthesize the initial composite, the stability of the preexisting ω is uncertain.

In FSW, a weld tool, consisting of a pin and shoulder, is rotated and plunged into the panel thickness, and traversed the length of the work piece, and hereby joining the material.[13,14] The two sides of the weld joint are

*Corresponding author. Email: jbc251@msstate.edu

referred to as the advancing side (AS), the side where tool rotation aligns with the travel direction, and the retreating side (RS), the side where tool rotation is opposite the travel direction. While the literature reports the use of FSW to join dissimilar alloys in butt and lap welds, these studies address the joining of different homogenous bulk material on either side of the weld.[15–17] This study investigates FSW as a possible joining method for a multi-layered, nano-scaled bimetal composite where both phases are resistant to chemical intermixing due to their positive heats of mixing in the solid phase.

FSW were made in a nominal 0.6 mm thick sheet of ARB Cu–Nb. The ARB material began with a single 2 mm thick sheet of polycrystalline Nb (99.97% pure, ATI-Wah Chang, Albany, OR) and two 1 mm thick sheets of polycrystalline Cu (99.99% pure, Southern Copper and Supply). The Nb layer was sandwiched between the two Cu layers and a 60% reduction in overall thickness was performed in a single step utilizing a two-high rolling mill (Waterbury-Farrel, Brampton, Canada). Layer thickness was reduced and number of layers increased through a repetitive sequence of cutting, stacking, and roll bonding. Prior to each roll bonding step, a surface treatment consisting of a 5-min ultrasonic acetone bath was performed followed by wire brushing. Further details of the ARB process can be found in the literature.[9,10] This process was repeated until a panel consisting of 50 vol.% Cu/50 vol.% Nb of alternating layers with average $h \approx 300$ nm was fabricated. A single piece, smooth tapered FSW tool was made from a lanthanated tungsten W-La_2O_3 alloy with a flat 2 mm diameter shoulder, initial pin length of 0.5 mm, upper diameter of 1 mm, and a taper of 27°mm. All FSWs were made in a bead on plate configuration using displacement control at a travel rate of 25.4 mm/m and a tool rotation of 1500 rpm.

Microstructure images were obtained using an FEI (Hillsboro, OR) Inspect F scanning electron microscope (SEM) and a FEI TITAN 300 keV transmission electron microscope (TEM). Hardness data were obtained on a Nano-XP 30 Indenter (Agilent, Santa Clara, CA) with a nominal 150 nm radius Berkovich tip. Load vs. displacement data were collected in continuous stiffness monitoring mode for indentation depths between 200 and 1100 nm and these data were used for hardness calculations.[18] The FSW panels were cross-sectioned normal to the welding direction using a low-speed diamond saw. SEM/indentation samples were mounted in a low heat epoxy resin and metallurgically ground and polished. TEM foils were extracted and thinned utilizing a FEI Helios focused ion beam (FIB).

Figure 1 shows a representative SEM-based secondary electron image (SEI) of a transverse section of the FSW. Regions of interest include the parent material (PM), the thermal mechanical affected zone (TMAZ), and the weld nugget (WN). All FSW, regardless of process parameters, exhibited a weld defect on the AS crown surface. The images in Figure 2 document the change in layer direction and thickness within the TMAZ region. Details of the representative regions in Figure 1 are shown in the SEI in Figure 2(a)–(c). Superimposed on these images are the nanohardness data with values in GPa. To resolve the finer layers, TEM bright field imaging (BFI), on the RS, was used to obtain Figure 2(d). It shows layers with an h of 6 nm, and a variation in material flow resulting from the asymmetrical flow field of the FSW.[13]

FIB was used to extract an additional foil from the region labeled by vertical red line in Figure 2(a). Figure 3 shows the higher magnification BFI TEM and accompanying ring selected area (electron) diffraction pattern (SADP), which indicates a nanocrystalline structure. Changes in diffraction contrast in the BFI TEM indicate an equiaxed grain structure approximately 5–10 nm in diameter. The ring SADP in Figure 3 confirms a nanocrystalline structure, which exhibits distinct Cu and Nb phases. The mottled contrast suggests that the individual phases are randomly distributed. The equiaxed grains

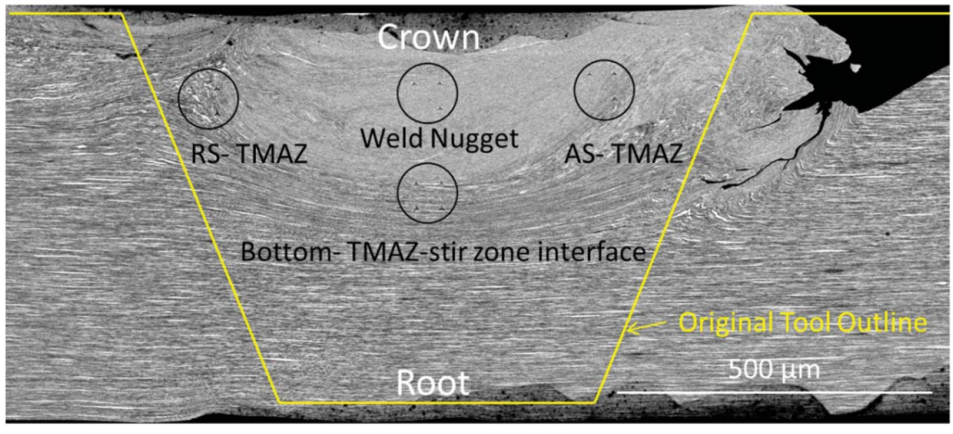

Figure 1. SEI of a transverse section of FSW with regions-of-interest marked. Note this sample was taken after 5 cm of travel with significant tool wear having occurred.

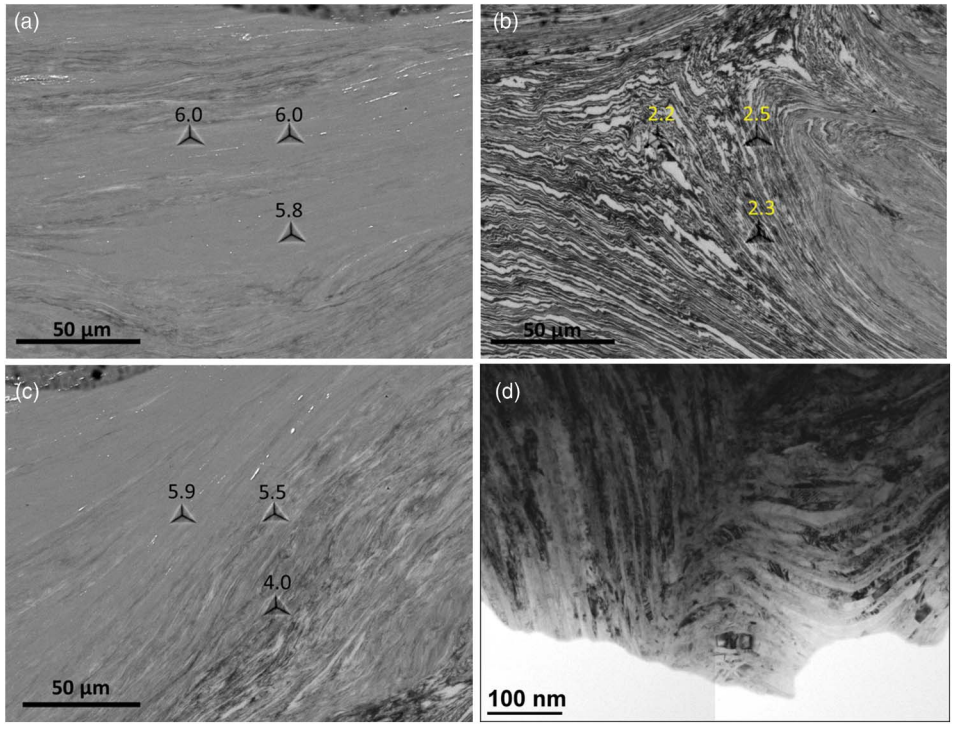

Figure 2. Details of FSW transverse seen in Figure 1. (a) FSW nugget, (b) RS TMAZ, and (c) AS TMAZ. Location of nanoindentations and hardness values in GPa are shown in (a)–(c) with (d) representing a BFI TEM of the RS WN in a layered region. The red line in (a) indicates the location where the TEM foil was extracted for Figure 3.

on the order of the refined h suggest a pinch-off mechanism may be responsible for the grain refinement.[19] In this mechanism, the torsional motion of the FSW process causes the sub-boundaries extending across the thickness of the elongated grains to pinch-off forming equiaxed grains.

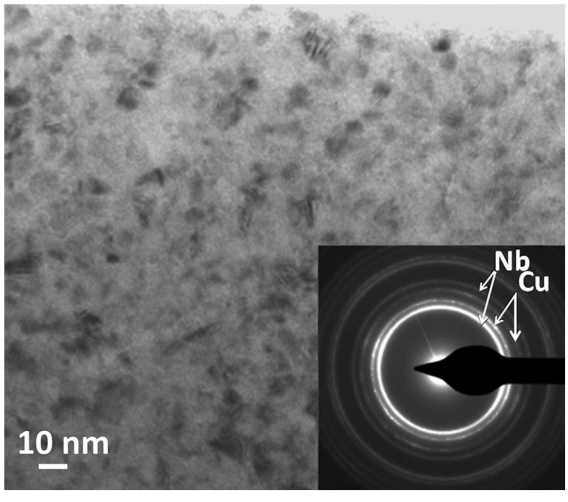

Figure 3. BFI TEM of WN exhibiting a nanocrystalline structure with equiaxed grains on the order of 5–10 nm in diameter. The inset accompanying SADP shows a ring structure, consistent with a polycrystalline grains, and the presence of both Cu and Nb phases.

The layered structure of the PM was maintained in parts of the FSW region as shown in Figure 2, especially on the RS and show changes in orientation resulting from the asymmetric material flow. Figure 2(d) shows a refined layered structure in the WN region, with the majority of the layers ranging from 6 to 12 nm. Equation (1) can be used to calculate the true strain (ε_t) input in the layered regions, and, assuming layer thicknesses in Figure 3(d) (which was close to the equiaxed nanograin region) of $\geq$6 nm to be stable, a minimum true strain required to form the equiaxed nanograin structure can also be calculated. For Equation (1); t_1 is the initial h of the PM and t_2 is the final h within the FSW nugget.

$$\varepsilon_t = \ln\left(\frac{t_1}{t_2}\right). \tag{1}$$

Thus for the observed reduction of h from 300 to 6 nm, the FSW process input a minimum strain of 3.9 in the equiaxed nanograin WN region. While this strain value is similar to strain ranges reported in other FSW studies of aluminum,[20–22] other studies indicate that higher strains are possible which vary as a function of location.[13]

A 2.5 GPa with a standard deviation of 0.13 GPa average hardness value was obtained from the 18 nanoindentations within the PM. Within the FSW region, the hardness values varied with respect to the refinement in microstructure. A steep increase in hardness was

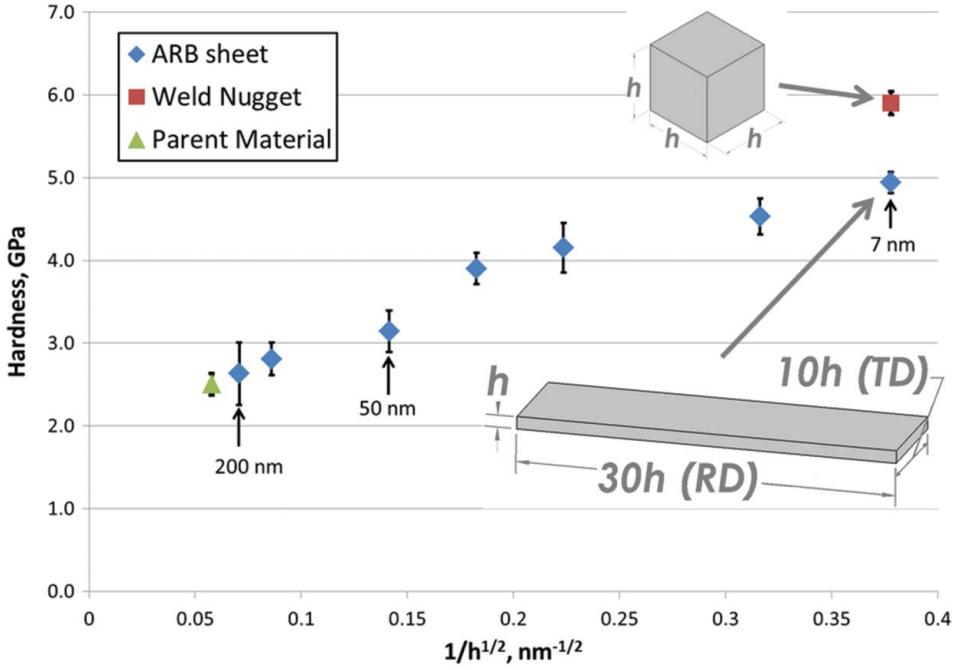

Figure 4. Hardness $v1/h^{1/2}$ plot for ARB Cu–Nb,[5] across length scales from the PM to the FSW WN. The insets illustrate the difference between the grains of an as rolled ARB panel (elongated grains) and the WN (equiaxed grains) at the finest length scale. Grain dimensions for the ARB panel are estimated from the literature.[10]

observed in the TMAZ region, due to the gradient of h. The average hardness of 5.9 GPa was measured in the equiaxed grain region of the WN.

The nanoindentation results performed on multiple FSW showed increases in hardness as ρ increases, consistent with observations from ARB Cu–Nb sheet material.[5,6,10] Figure 4 plots Cu–Nb ARB hardness vs. $h^{1/2}$ across the length scale from the PM to the FSW WN.[5] It also illustrates the difference in grain geometry between the WN and an as rolled ARB panel.[5]

Figure 4 shows a 20% increase in hardness in the equiaxed 7 nm grain size region of the WN compared to that of the an ARB panel with $h = 7$ nm. This increase in hardness likely arises due to different deformation mechanisms in the equiaxed grains of the WN.[23–28] Increased hardness suggests that friction-stir processing of Cu–Nb plates could be used to form a three-dimensional (3D) nanocrystalline structure to further increase the maximum obtainable strength. The significance in a 20% increase in hardness over an already extremely hard material (considering its bulk counterparts) could be of particular importance in high wear applications, and other areas where an even further increase in surface, or through-thickness, hardness is desired.

Although resolvable with TEM, the small size presented by the grains precluded an electron backscatter diffraction study of ω within the WN. Studies of ARB sheets had well-defined layer directions, which allowed the use of a normal direction inverse pole figure to act as a measure of the interface plane normal distribution. With no layer directions present in the WN, bulk texture measurements via neutrons or X-rays will not provide an understanding of ω. With grain diameters on the order of 7 nm, this also limits the applicability of local texture measurements such as precession electron diffraction within a TEM, a technique used in the past for investigations of Cu–Nb nanoscale multi-layers.[29,30]

With regards to the FSW process, there was a defect on the AS of the FSW region. This type of defect is typically seen in FSW when the insufficient down-force is applied.[31] Although the shoulder was in contact with the material during welding, a substantial influence on the material flow from the shoulder was not observed as evidenced by the minimal material movement on the RS seen in Figure 1. Weld material on the AS, beyond the defect and not shown in Figure 1, was also in intimate contact with the shoulder, but material-movement/shoulder-interaction was virtually nonexistent. It is possible that adding features to the shoulder would help increase the lateral material-movement and help eliminate the volumetric defect.[14]

Tool wear during welding was significant with pin length decreasing by 50% after 5 cm of FSW length. Different material selections for the tool should improve tool life and preserve features added to improve material flow. Although improvements in tool life and preventing defect formations are still areas of concern, FSW seems to be a viable option for joining this type of material while maintaining its enhanced strength.

FSW of the ARB panels lead to both refined layers, and a nanocrystalline structure. Where layers were present, directional changes were observed due to the non-symmetric flow field of the FSW.[32,33] The initial h of 300 nm was reduced to grains with 3D nanoscale diameters of 7 nm following the FSW process. Within the WN hardness values of the equiaxed grain region exceeded those of ARB Cu–Nb panels with h equal to the equiaxed grain diameter. Hardness values were noted to increase from 2.5 GPa in the starting PM and increased to a maximum of 6.0 GPa as the length scale decreased.

Acknowledgements This work is supported by the Los Alamos National Laboratory Directed Research and Development (LDRD) project 20130764ECR. This work was performed, in part, at the Center for Integrated Nanotechnologies, an Office of Science User Facility operated for the U.S. Department of Energy (DOE) Office of Science. Los Alamos National Laboratory, an affirmative action equal opportunity employer, is operated by Los Alamos National Security, LLC, for the National Nuclear Security Administration of the US Department of Energy under contract DE-AC52-06NA25396. Electron microscopy was performed at the Los Alamos Electron Microscopy Laboratory.

References

[1] Mara NA, Bhattacharyya D, Dickerson P, Hoagland RG, Misra A. Deformability of ultrahigh strength 5 nm Cu/Nb nanolayered composites. Appl Phys Lett. 2008;92(23):231901.

[2] Misra A, Hirth JP, Hoagland RG. Length-scale-dependent deformation mechanisms in incoherent metallic multi-layered composites. Acta Mater. 2005;53(18):4817–4824.

[3] Misra A, Demkowicz MJ, Zhang X, Hoagland RG. The radiation damage tolerance of ultra-high strength nanolayered composites. JOM. 2007;59(9):62–65.

[4] Han W, Demkowicz MJ, Mara NA, Fu E, Sinha S, Rollett AD, Wang Y, Carpenter JS, Beyerlein IJ, Misra A. Design of radiation tolerant materials via interface engineering. Adv Mater. 2013;25(48):6975–6979.

[5] Beyerlein IJ, Mara NA, Carpenter JS, Nizolek T, Mook WM, Wynn TA, McCabe RJ, Mayeur JR, Kang K, Zheng S, Wang J, Pollock TM. Interface-driven microstructure development and ultra high strength of bulk nanostructured Cu–Nb multilayers fabricated by severe plastic deformation. J Mater Res. 2013;28(13):1799–1812.

[6] Carpenter JS, Zheng SJ, Zhang RF, Vogel SC, Beyerlein IJ, Mara NA. Thermal stability of Cu–Nb nanolamellar composites fabricated via accumulative roll bonding. Philos Mag. 2013;93(7):718–735.

[7] Zheng S, Beyerlein IJ, Carpenter JS, Kang K, Wang J, Han W, Mara NA. High-strength and thermally stable bulk nanolayered composites due to twin-induced interfaces. Nat Commun. 2013;4, Article number 1696. doi: 10.1038/ncomms2651.

[8] Lee S-B, LeDonne JE, Lim SCV, Beyerlein IJ, Rollett AD. The heterophase interface character distribution of physical vapor-deposited and accumulative roll-bonded Cu–Nb multilayer composites. Acta Mater. 2012;60(4):1747–1761.

[9] Carpenter JS, Vogel SC, LeDonne JE, Hammon DL, Beyerlein IJ, Mara NA. Bulk texture evolution of Cu–Nb nanolamellar composites during accumulative roll bonding. Acta Mater. 2012;60(4):1576–1586.

[10] Carpenter JS, McCabe RJ, Vogel SC, Rollett AD, Mara NA, Beyerlein IJ. Process parameter influence on texture evolution in Cu–Nb multilayer composites fabricated via accumulative roll bonding. Met Mater Trans. A 2014. doi:10.1007/s11661-013-2162-4

[11] Bronkhorst CA, Mayeur JR, Beyerlein IJ, Mourad HM, Hansen BL, Mara NA, Carpenter JS, McCabe RJ, Sintay SD. Meso-scale modeling the orientation and interface stability of Cu/Nb-layered composites by rolling. JOM. 2013;65(3):431–442.

[12] Hansen BL, Carpenter JS, Sintay SD, Bronkhorst CA, McCabe RJ, Mayeur JR, Mourad HM, Beyerlein IJ, Mara NA, Chen SR, Gray III GT. Modeling the texture evolution of Cu/Nb layered composites during rolling. Int J Plast. 2013;49:71–84.

[13] Schneider JA, Nunes, AC, Jr. Characterization of plastic flow and resulting microtextures in a friction stir weld. Metall Mater Trans B. 2004;35(4):777–783.

[14] Mishra RS, Ma ZY. Friction stir welding and processing. Mater Sci Eng R Rep. 2005;50(1–2):1–78.

[15] Schneider C, Weinberger T, Inoue J, Koseki T, Enzinger N. Characterisation of interface of steel/magnesium FSW. Sci Technol Weld Join. 2011;16(1):100–107.

[16] Galvão I, Leal RM, Loureiro A, Rodrigues DM. Material flow in heterogeneous friction stir welding of aluminium and copper thin sheets. Sci Technol Weld Join. 2010;15(8):654–660.

[17] Sun YF, Fujii H, Takaki N, Okitsu Y. Microstructure and mechanical properties of dissimilar Al alloy/steel joints prepared by a flat spot friction stir welding technique. Mater Des. 2013;47:350–357.

[18] Oliver WC, Pharr GM. Measurement of hardness and elastic modulus by instrumented indentation: advances in understanding and refinements to methodology. J Mater Res. 2004;19(01):3–20.

[19] Doherty RD, Hughes DA, Humphreys FJ, Jonas JJ, Jensen DJ, Kassner ME, King WE, McNelley TR, McQueen HJ, Rollett AD. Current issues in recrystallization: a review. Mater Sci Eng A. 1997;238(2):219–274.

[20] Arora A, Zhang Z, De A, DebRoy T. Strains and strain rates during friction stir welding. Scripta Mater. 2009;61(9):863–866.

[21] Chen ZW, Cui S. Strain and strain rate during friction stir welding/processing of Al–7Si–0.3Mg alloy. IOP ConfSer Mater Sci Eng. 2009;4(1):012026.

[22] Buffa G, Hua J, Shivpuri R, Fratini L. A continuum based FEM model for friction stir welding—model development. Mater Sci Eng A. 2006;419(1–2):389–396.

[23] Yang W, Wang H. Mechanics modeling for deformation of nano-grained metals. J Mech Phys Solids. 2004;52(4):875–889.

[24] Van Swygenhoven H, Caro A, Farkas D. A molecular dynamics study of polycrystalline fcc metals at the nanoscale: grain boundary structure and its influence on plastic deformation. Mater Sci Eng A. 2001;309–310:440–444.

[25] Fu H-H, Benson DJ, Meyers MA. Analytical and computational description of effect of grain size on yield stress of metals. Acta Mater. 2001;49(13):2567–2582.

[26] Yamakov V, Wolf D, Phillpot SR, Mukherjee AK, Gleiter H. Dislocation processes in the deformation of nanocrystalline aluminium by molecular-dynamics simulation. Nat Mater. 2002;1(1):45–49.

[27] Meyers MA, Mishra A, Benson DJ. Mechanical properties of nanocrystalline materials. Prog Mater Sci. 2006;51(4):427–556.
[28] Raj R, Ashby MF. On grain boundary sliding and diffusional creep. Metall Trans. 1971;2(4):1113–1127.
[29] Carpenter JS, Liu X, Darbal A, Nuhfer NT, McCabe RJ, Vogel SC, LeDonne JE, Rollett AD, Barmak K, Beyerlein IJ, Mara NA. A comparison of texture results obtained using precession electron diffraction and neutron diffraction methods at diminishing length scales in ordered bimetallic nanolamellar composites. Scripta Mater. 2012;67(4):336–339.
[30] Liu X, Nuhfer NT, Rollett AD, Sinha S, Lee S-B, Carpenter JS, LeDonne JE, Darbal A, Barmak K. Interfacial orientation and misorientation relationships in nanolamellar Cu/Nb composites using transmission-electron-microscope-based orientation and phase mapping. Acta Mater. 2014;64:333–344.
[31] Kim YG, Fujii H, Tsumura T, Komazaki T, Nakata K. Three defect types in friction stir welding of aluminum die casting alloy. Mater Sci Eng A. 2006;415(1–2):250–254.
[32] Murr LE, Li Y, Flores RD, Trillo EA, McClure JC. Intercalation vortices and related microstructural features in the friction-stir welding of dissimilar metals. Mater Res Innov. 1998;2(3):150–163.
[33] Li Y, Murr LE, McClure JC. Solid-state flow visualization in the friction-stir welding of 2024 Al to 6061 Al. Scripta Mater. 1999;40(9):1041–1046.